



Quasiparticle states for integer- and fractional-charged electron wave packetsX. K. Yue and Y. Yin ^{*}*Department of Physics, Sichuan University, Chengdu, Sichuan 610065, China* (Received 30 June 2020; revised 9 June 2021; accepted 9 June 2021; published 22 June 2021)

It is well known that Lorentzian voltage pulses with integer quantum flux can inject integer-charged wave packets without electron-hole pairs. The wave packets are composed of solitonlike quasiparticles on top of the Fermi sea, which have been named “levitons.” However, it is not clear what kind of charged quasiparticles can be injected by Lorentzian pulses with fractional quantum flux. To answer this question, we study the wave packets injected by a train of Lorentzian pulses with repetition period T . We introduce a set of one-body wave functions, within which the quantum state of the charged quasiparticles can be described for pulses with arbitrary quantum flux. We find that in the general case, the injection of the charged quasiparticles is characterized by two different timescales: one is decided by the repetition period T of the pulse train, while the other one is T rescaled by a factor related to the flux of the pulses. For pulses with integer quantum flux, the two timescales match each other. In this case, the charged quasiparticles are levitons, which are injected with a single period T . For pulses with fractional quantum flux, the two timescales mismatch. The charged quasiparticles can then be injected in a multiperiodic way. This makes each quasiparticle carry only a fractional electric charge into the quantum conductor within a single period T . These quasiparticles can have pronounced impact on the charge injection. In particular, they can lead to the cycle-missing event, in which the voltage pulse fails to inject an electron within a single period T . The cycle-missing event can be seen intuitively from the waiting time distribution between electrons above the Fermi sea, which exhibits a series of peaks at multiples of the period T . By using the wave functions of the charged quasiparticles, we elucidate in detail how a leviton evolves as the flux of the pulse changes. In the meantime, we also clarify how additional eh pairs can be excited.

DOI: [10.1103/PhysRevB.103.245429](https://doi.org/10.1103/PhysRevB.103.245429)**I. INTRODUCTION**

In the past decade, much effort has been devoted to the on-demand single-electron source, within which electron wave packets carrying single or few electric charges can be injected coherently into a quantum conductor [1–20]. In a simple way, such injection can be realized by applying a nanosecond pulse on the Ohmic contact of the conductor, as illustrated in Fig. 1. The injected charges Q of the wave packet are decided by the flux φ of the pulse, while the detailed quantum state of the wave packet can be controlled via fine tuning the profile of the pulse. This offers a simple but feasible approach to archive the time-resolved quantum control of propagating electron wave packet in solid-state circuits [21–34].

Generally speaking, the wave packet is composed of charged quasiparticles in the Fermi sea (\mathbf{F}) of the conductor, which are usually accompanied by a neutral cloud of electron-hole (eh) pairs [35,36]. Remarkably, it is possible to inject a “clean” wave packet without eh pairs, which can be done by tuning the pulse to be a Lorentzian with integer quantum flux [3,37]. In doing so, one obtains solitonlike quasiparticles propagating on top of the Fermi sea, which have been named “levitons” [2,8]. Each leviton carries a unit electric charge and has a well-defined wave function. By using a train of

Lorentzian pulses, a sequence of levitons can be injected into a quantum conductor. The corresponding wave functions can be obtained via quantum state tomography [8,34,38–40]. This makes levitons promising candidates for flying qubits in solid-state circuits [41–45].

By using a Lorentzian pulse with fractional quantum flux, one can inject a wave packet carrying fractional charges, which has a quite different structure. On one hand, it contains a large amount of eh pairs. These eh pairs can lead to a strong fluctuations of the injected charges, which is closely related to the dynamical orthogonality catastrophe [46,47]. On the other hand, it can sustain single-particle excitations, which behave like quasiparticles carrying effectively fractional charges. The structure of the wave packet has been demonstrated for the Lorentzian pulse with a half-quantum flux. In this case, the quantum state of the wave packet can be decomposed into two mixed states: one represents the neutral cloud of eh pairs, while the other one can be regarded as a zero-energy quasiparticle carrying an effectively $e/2$ charge [48]. This makes the wave packet show distinctly different features from the wave packet built from levitons [27,49,50].

Intuitively, one expects that the fractional-charged single-particle excitations can be injected in a similar way as levitons, providing an alternative approach to realize flying qubits. However, the nature of these single-particle excitations has not been fully understood. In particular, it is not clear how a leviton can evolve into a fractional-charged single-particle excitation as the flux of pulses changes. To answer this question,

^{*}Author to whom correspondence should be addressed: yin80@scu.edu.cn

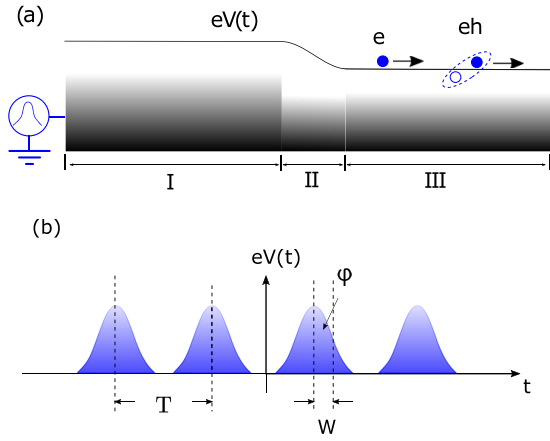


FIG. 1. (a) Schematic of the on-demand electron injection via the voltage pulse $V(t)$. By applying $V(t)$ on the contact of the quantum conductor, electron (hole) or eh pairs from the reservoir (region I) can be injected into the quantum conductor (region III). The voltage drop is assumed to occur across a short interval at the interface (region II). (b) Schematics of the applied voltage pulses, which form a pulse train with repetition period T . Each pulse can be characterized by half-width at half-maximum W and Faraday flux ϕ .

one needs to describe the quantum states for both integer- and fractional-charged wave packets in a unified manner, which has not been given yet.

In this paper, we attack this problem by examining the case when a Lorentzian pulse train with repetition period T is applied on the Ohmic contact, as illustrated in Fig. 1(b). In this case, the charge Q injected within a single period T can be solely decided by the flux ϕ of the Lorentzian pulse as $Q = e\phi$. We show that the injected charges are carried by a train of wave packets, whose quantum state can be given as

$$|\Psi_{\text{train}}\rangle = \prod_{l=0, \pm 1, \pm 2, \dots} |\Psi_l\rangle, \quad (1)$$

with $|\Psi_l\rangle$ representing the quantum state of the l th wave packet. Each wave packet is composed of charged quasiparticles and neutral eh pairs, which can be described by a set of one-body wave functions $\psi_{kl}^\alpha(t)$, with $\alpha = c$ for the quasiparticles and $\alpha = e/h$ for the electron and hole component of the eh pairs. This allows one to introduce the corresponding creation operators

$$\begin{aligned} C_{kl}^\dagger &= \int_{-\infty}^{+\infty} dt \psi_{kl}^c(t) \hat{a}^\dagger(t), \\ (B_{kl}^e)^\dagger &= \int_{-\infty}^{+\infty} dt \psi_{kl}^e(t) \hat{a}^\dagger(t), \\ (B_{kl}^h)^\dagger &= \int_{-\infty}^{+\infty} dt \psi_{kl}^h(t) \hat{a}(t), \end{aligned} \quad (2)$$

with $\hat{a}(t)$ [$\hat{a}^\dagger(t)$] being the electron annihilation (creation) operator in the time domain. In doing so, the quantum state of the l th wave packet can be described by the Slater determinant as

$$|\Psi_l\rangle = \left[\prod_k C_{kl}^\dagger \right] \prod_k [\sqrt{1-p_k} + i\sqrt{p_k} (B_{kl}^e)^\dagger (B_{kl}^h)^\dagger] |\mathbf{F}\rangle, \quad (3)$$

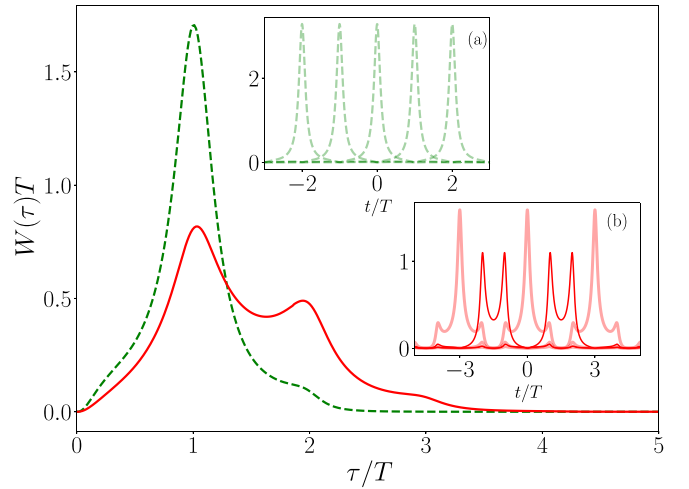


FIG. 2. The waiting time distribution $W(\tau)$ between electrons above the Fermi sea (main panel) and the corresponding wave function $\psi_{kl}^\alpha(t)$ (inset), corresponding to the pulse width $W/T = 0.1$. The green dashed curve in the inset (a) represent the wave functions of levitons, corresponding to $Q/e = 1$. The red solid curves in the inset (b) represent the wave functions of the charged quasiparticles, corresponding to $Q/e = \frac{2}{3}$. Note that there are two types of quasiparticles here, which are represented by the thick and thin curves.

with p_k representing the excitation probabilities of the eh pairs. Both the excitation probabilities p_k and the one-body wave functions $\psi_{kl}^\alpha(t)$ can be extracted from the time-dependent scattering matrix, providing a general way to study the quantum state of both the integer- and fractional-charged wave packets.

As the charges Q are injected with the period T , one may expect that the charged quasiparticles are also injected with the same period. Indeed, this picture holds when Q/e takes integer values. This is illustrated in the inset (a) of Fig. 2, corresponding to $Q/e = 1$. In this case, all the one-body wave functions of the charged quasiparticles exhibit the same profiles, which are separated from each other by the time interval T . They essentially correspond to a periodic train of levitons. The structure of the leviton train can be understood intuitively from the corresponding waiting time distribution $W(\tau)$ (WTD) [51], which is characterized by a strong peak around $\tau = T$ (see the green dashed curve in the main panel of Fig. 2). This indicates that the voltage pulse tends to inject exactly one electron per period into the quantum conductor.

In contrast, the above picture is inapplicable when Q/e takes fractional values. In this case, the injection of the charged quasiparticles is essentially characterized by two different timescales: one is decided by the repetition period T , while the other one is T rescaled by a factor related to Q/e . Due to the mismatch between these two timescales, the charge quasiparticles are injected in a multiperiodic way. This makes the corresponding wave functions exhibit different profiles, which are injected with an extended period longer than T . This is illustrated in the inset (b) of Fig. 2, corresponding to $Q/e = \frac{2}{3}$. One can see that the wave functions can exhibit two types of profiles, which are plotted with thick and thin curves. They are separated from each other by the time interval $3T/2$. On average, each quasiparticle can carry only $2e/3$ charge

into the quantum conductor within a single period T . This makes them behave *effectively* like quasiparticles carrying fractional charges. These quasiparticles can have pronounced impact on the charge injection. In particular, they lead to the cycle-missing event, in which the voltage pulse can fail to inject an electron within a single period T . Such event can be seen from the corresponding WTD $W(\tau)$, which exhibits a series of peaks at multiples of the period T (see the red solid curve in Fig. 2).

The wave function $\psi_{kl}^c(t)$ can provide a unified description of the charged quasiparticles, which is applicable for both the integer- and fractional-charged wave packets. This allows us to elucidate in detail how a leviton evolves as the flux φ of the pulse changes. In the meantime, our approach can also provide the information of the eh pairs. This allows us to clarify how additional eh pairs can be excited during the evolution of the levitons.

The paper is organized as follows: In Sec. II, we present the model of the system and introduce a general expression for the quantum state of the wave packets. We discuss the typical behaviors of the wave functions of quasiparticles in Secs. III and IV. The corresponding waiting time distribution is also discussed in these two sections. The evolution of levitons and eh pairs is discussed in Secs. V and VI, respectively. We summarize our findings in Sec. VII.

II. BLOCH-MESSIAH REDUCTION IN THE FRAMEWORK OF SCATTERING MATRIX FORMALISM

The electron source can be modeled as a single-mode quantum conductor, as illustrated in Fig. 1(a). We choose the driving voltage $V(t)$ of the form

$$\frac{e}{\hbar}V(t) = \sum_{l=0,\pm 1,\pm 2,\dots} \frac{2\varphi W}{W^2 + (t-lT)^2}, \quad (4)$$

which corresponds to a periodic train of Lorentzian pulses with width W [see Fig. 1(b)]. The voltage drop $V(t)$ between the contact and the conductor is assumed to occur across a short interval, so that the corresponding dwell time τ_D satisfies $k_B T_e \ll \hbar/T < \hbar/W \ll \hbar/\tau_D \ll E_F$, with E_F representing the Fermi energy and T_e representing the electron temperature. In this paper, we choose $E_F = 0$ and concentrate on the zero-temperature limit.

The scattering matrix of the system can be solely determined by the driving voltage $V(t)$ as

$$S(t, t') = \delta(t - t') \exp \left[-i \frac{e}{\hbar} \int_0^t d\tau V(\tau) \right]. \quad (5)$$

Given the scattering matrix, the electrons in the contact and the conductor can be related via the equation

$$\hat{b}(t) = \int dt' S(t, t') \hat{a}(t'), \quad (6)$$

where $\hat{a}(t)$ and $\hat{b}(t)$ represent the electron annihilation operators in the Ohmic contact and the quantum conductor, respectively.

In this setup, the injected current can be simply given as $I(t) = (e^2/h)V(t)$. The charge Q injected within a single period is determined solely by the flux φ as

$$Q = \int_{-T/2}^{+T/2} dt I(t) = e\varphi. \quad (7)$$

For simplicity, here we assume $Q/e > 0$ so that the wave packets carry negative charges.

In the absence of interactions, the quantum state of the injected wave packets can be obtained from the Bloch-Messiah reduction, which extracts the many-body quantum state from the decomposition of the excess one-body correlation function $G_{ex}(t, t')$ [38,52,53]. In the zero-temperature limit, $G_{ex}(t, t')$ can be given as

$$iG_{ex}(t, t') = \langle \mathbf{F} | [\hat{b}^\dagger(t') \hat{b}(t) - \hat{a}^\dagger(t') \hat{a}(t)] | \mathbf{F} \rangle, \quad (8)$$

with $|\mathbf{F}\rangle$ representing the Fermi sea. To find the many-body state corresponding to $G_{ex}(t, t')$, the Bloch-Messiah reduction essentially seeks out the quantum state $|\Psi\rangle$, which satisfies

$$\langle \Psi | \hat{a}^\dagger(t') \hat{a}(t) | \Psi \rangle = \langle \mathbf{F} | \hat{b}^\dagger(t') \hat{b}(t) | \mathbf{F} \rangle. \quad (9)$$

This can be done by a proper decomposition of $G_{ex}(t, t')$ [54,55]. Here we only present the outline and leave the details to Appendix A.

A. Decomposition in Floquet space

For the system under periodic driving, it is straightforward to perform such decomposition in Floquet space [56,57], which can be generally written as

$$iG_{ex}(t, t') = \sum_k \int_0^\Omega \frac{d\omega}{\Omega} e^{-i\omega(t-t')} u_k^c(\omega, t) [u_k^c(\omega, t')]^* + \sum_k \int_0^\Omega \frac{d\omega}{\Omega} e^{-i\omega(t-t')} [u_k^e(\omega, t), u_k^h(\omega, t)] \times \begin{bmatrix} p_k(\omega) & i\sqrt{p_k(\omega)[1-p_k(\omega)]} \\ -i\sqrt{p_k(\omega)[1-p_k(\omega)]} & -p_k(\omega) \end{bmatrix} \begin{bmatrix} u_k^e(\omega, t') \\ u_k^h(\omega, t') \end{bmatrix}^*, \quad (10)$$

with the asterisk denoting the complex conjugation. In the above expression, the quantity $p_k(\omega)$ is real, which satisfies $p_k(\omega) \in [0, 1]$. The functions $u_k^\alpha(\omega, t)$ are complex, which are periodic in the time domain $u_k^\alpha(\omega, t) = u_k^\alpha(\omega, t + T)$ with $\alpha = c, e, \text{ and } h$. These functions can form an orthonormal

basis within a single period, i.e.,

$$\int_{-T/2}^{T/2} dt [u_{k'}^{\alpha'}(\omega, t)]^* u_k^\alpha(\omega, t) = \delta_{\alpha, \alpha'} \delta_{k, k'}. \quad (11)$$

TABLE I. Parameter space for $k = [n, m]$ for the charged quasiparticles ($\alpha = c$) and eh pairs ($\alpha = e, h$), corresponding to $n, m \leq 3$. The parameters for the charged quasiparticles are marked in gray shadow.

[0, 0]	[1, 0]	[2, 0]	[3, 0]
[0, 1]	[1, 1]	[2, 1]	[3, 1]
[0, 2]	[1, 2]	[2, 2]	[3, 2]
[0, 3]	[1, 3]	[2, 3]	[3, 3]

All these functions can be characterized by two indices ω and k . Here k is a discrete index, which can be described by (dimensionless) integer numbers. In contrast, the index ω has the unit of frequency, which satisfies $\omega \in [0, \Omega)$ with $\Omega = 2\pi/T$ being the repetition rate of the pulses.

The function $u_k^\alpha(\omega, t)$ is closely related to the one-body wave function of the charged quasiparticle ($\alpha = c$) and the neutral eh pair ($\alpha = e, h$), while $p_k(\omega)$ represents the excitation probability of the eh pair. Both $u_k^\alpha(\omega, t)$ and $p_k(\omega)$ can be obtained from the polar decomposition of the scattering matrix. In general cases, they can exhibit a complicated dependence on ω . For the scattering matrix given in Eq. (5), we find that the ω dependence can be much simpler: First, the probabilities $p_k(\omega)$ are independent on ω and can hence be written as p_k for short. Second, $u_k^\alpha(\omega, t)$ can be written in the form of separation of variables as

$$u_k^\alpha(\omega, t) = U_k^\alpha(t)F_k^Q(\omega), \quad (12)$$

where $F_k^Q(\omega)$ is a real function defined in the region $\omega \in [0, \Omega)$, while $U_k^\alpha(t)$ is a complex periodic function defined in the whole time domain $t \in (-\infty, +\infty)$, which satisfies $U_k^\alpha(t) = U_k^\alpha(t + T)$.

The function $U_k^\alpha(t)$ usually has to be obtained numerically, which is sensitive to the details of the scattering matrix. In contrast, the function $F_k^Q(\omega)$ can be given analytically. To do this, it is convenient to describe the discrete index k by two non-negative integers n and m [i.e., $n, m = 0, 1, 2, \dots$] [see Eqs. (A14), (A15), and (A16) in Appendix A for details]. In doing so, we find that $F_k^Q(\omega)$ can be written as

$$F_k^Q(\omega) = \begin{cases} H[(Q/e - n + 1)\Omega - \omega] & \text{for } Q/e \in [n - 1, n], \\ H[\omega - (Q/e - n)\Omega] & \text{for } Q/e \in (n, n + 1], \\ 0 & \text{otherwise} \end{cases} \quad (13)$$

with $H(\omega)$ representing the Heaviside step function.¹ Note that $F_k^Q(\omega)$ is independent on the details of the scattering matrix and is solely decided by the charge Q of the wave packet.

It is worth noting that the available parameter space of the index $k = [n, m]$ is different for the charged quasiparticles ($\alpha = c$) and the eh pairs ($\alpha = e, h$): one has $m < n$ for the charged quasiparticles, while $m \geq n$ for the eh pairs. This can be demonstrated more intuitively in Table I.

B. Decomposition in wave-packet representation

Given the decomposition of $G_{ex}(t, t')$ in Eq. (10), one can construct a set of one-body wave functions corresponding to the injected quasiparticles. The many-body state of the wave packets can then be described by using the Slater determinant built from them. However, one can construct different sets of one-body wave functions, which are related to each other via unitary transformations. Hence, the detailed expression of the Slater determinant is not uniquely defined. As the driving voltage $V(t)$ corresponds to a train of pulses [see Eq. (4)], it is favorable to express the one-body wave functions in a similar form. This can be done by defining a set of wave functions $\psi_{kl}^\alpha(t)$ from $u_k^\alpha(\omega, t)$ as

$$\begin{aligned} \psi_{kl}^\alpha(t) &= \frac{1}{\sqrt{q_k}} \int_0^\Omega \frac{d\omega}{\Omega} e^{-i\omega(t - lT/q_k)} u_k^\alpha(\omega, t) \\ &= U_k^\alpha(t) \int_0^\Omega \frac{d\omega}{\Omega} \frac{F_k^Q(\omega)}{\sqrt{q_k}} e^{-i\omega(t - lT/q_k)}, \end{aligned} \quad (14)$$

with $l = 0, \pm 1, \pm 2, \dots$. Note that we have introduced a normalization factor q_k so that $\psi_{kl}^\alpha(t)$ can form an orthonormal basis set in the whole time domain $t \in (-\infty, +\infty)$, which satisfies

$$\int_{-\infty}^{+\infty} dt [\psi_{k'l'}^{\alpha'}(t)]^* \psi_{kl}^\alpha(t) = \delta_{\alpha, \alpha'} \delta_{k, k'} \delta_{l, l'}. \quad (15)$$

By substituting Eqs. (12), (13), and (14) into (15), it is straightforward to show that q_k can be given analytically as

$$q_k = q_{[n, m]} = \begin{cases} Q/e - n + 1 & \text{for } Q/e \in [n - 1, n], \\ n + 1 - Q/e & \text{for } Q/e \in (n, n + 1], \\ 0 & \text{otherwise.} \end{cases} \quad (16)$$

The wave functions $\psi_{kl}^\alpha(t)$ can be regarded as Martin-Landauer-type wave packets [58], which offers an intuitive way to interpret the time-resolved behavior of the charged quasiparticles ($\alpha = c$) and eh pairs ($\alpha = e, h$). The decomposition of $G_{ex}(t, t')$ can then be given as

$$\begin{aligned} iG_{ex}(t, t') &= \sum_{k, l} \psi_{kl}^c(t) [\psi_{kl}^c(t')]^* + \sum_{k, l} [\psi_{kl}^e(t), \psi_{kl}^h(t)] \\ &\quad \times \begin{bmatrix} p_k & i\sqrt{p_k[1 - p_k]} \\ -i\sqrt{p_k[1 - p_k]} & -p_k \end{bmatrix} \begin{bmatrix} \psi_{kl}^e(t') \\ \psi_{kl}^h(t') \end{bmatrix}^*. \end{aligned} \quad (17)$$

For wave packets carrying integer and fractional charges, both the charged quasiparticles and eh pairs can show different natures, leading to wave functions with different features. To better demonstrate these differences, we shall first concentrate on two concrete examples: wave packets carrying on average a unit ($Q = e$) and two-thirds ($Q/e = \frac{2}{3}$) electric charges per period.

III. WAVE PACKET WITH UNIT CHARGE

Let us start our discussion from the wave packets carrying on average a unit electric charge ($Q = e$) per period. In this

¹Here we choose $H(0) = 1$.

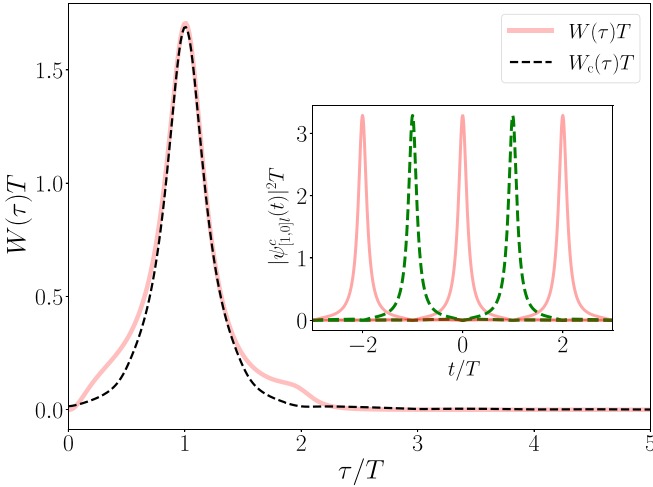


FIG. 3. The WTD between electrons above the Fermi sea, corresponding to the width $W/T = 0.1$. The red solid curve represents the exact WTD, while the black dashed curve represents the semiclassical approximation from Eq. (28). The corresponding train of levitons are illustrated by the wave functions $|\psi_{[1,0]l}^c(t)|^2 T$ in the inset. The red solid curves correspond to $l = -2, 0$, and 2 , while the green dashed curves correspond to $l = -1$ and 1 .

case, the decomposition of $G_{ex}(t, t')$ takes a simple form

$$iG_{ex}(t, t') = \sum_l \psi_{[1,0]l}^c(t) [\psi_{[1,0]l}^c(t')]^*. \quad (18)$$

This indicates that each wave packet contains only one charged quasiparticle associated with the index $k = [1, 0]$. By introducing the creation operator

$$C_{[1,0]l}^\dagger = \int_{-\infty}^{+\infty} dt \psi_{[1,0]l}^c(t) \hat{a}^\dagger(t), \quad (19)$$

the corresponding many-body state of the whole wave packet train can be expressed as

$$|\Psi_{\text{train}}\rangle = \prod_{l=0, \pm 1, \pm 2, \dots} C_{[1,0]l}^\dagger |\mathbf{F}\rangle. \quad (20)$$

Equation (20) essentially corresponds to a periodic train of levitons. Accordingly, the wave functions $\psi_{[1,0]l}^c(t)$ can be regarded as Martin-Landauer-type wave packets built from levitons. This can be seen more clearly by carrying out the integration in Eq. (14)²:

$$\psi_{[1,0]l}^c(t) = U_{[1,0]}^c(t) e^{-i\Omega(t-lT)/2} \text{sinc}\left[\frac{\Omega(t-lT)}{2\pi}\right], \quad (21)$$

with $\text{sinc}(t) = \sin(\pi t)/(\pi t)$ and the periodic function

$$U_{[1,0]}^c(t) = \frac{\sqrt{\cosh(\pi W/T) \sinh(\pi W/T)/T}}{\sin[\pi(t/T - iW/T)]} \quad (22)$$

represents the leviton train [40,53,59]. Each wave function $\psi_{[1,0]l}^c(t)$ exhibits a strong peak around $t = lT$, corresponding to a leviton injected in the l th period. Wave functions with different l can form a periodic sequence, providing an intuitive

way to understand the structure of the wave-packet train. This is illustrated in the inset of Fig. 3.

The wave functions $\psi_{[1,0]l}^c(t)$ can provide an orthonormal basis set in the time domain, within which various physical quantities can be expressed in a neat way. In particular, the current carried by the train of levitons can be written as (see Appendix B for details)

$$I(t) = \sum_{l=0, \pm 1, \pm 2, \dots} e |\psi_{[1,0]l}^c(t)|^2. \quad (23)$$

One notices that in Eq. (23), the current $I(t)$ is expressed as an incoherent summation of all the wave functions $\psi_{[1,0]l}^c(t)$, even if these functions can overlap with each other (see the inset of Fig. 3). However, this does not mean that levitons contribute incoherently to the charge transport process. In fact, the overlap between the wave functions can enhance the fluctuations of the waiting time between successive electron injection. This effect can be seen more intuitively from the waiting time distribution (WTD) between electrons above the Fermi sea [60–62].

The WTD can be calculated from the corresponding idle time probability $\Pi(t_s, t_e)$ [51]. It can be expressed as the determinant (see Appendix C for details)

$$\Pi(t_s, t_e) = \det[\hat{1} - \hat{Q}_{se}], \quad (24)$$

where $\hat{1}$ denotes the unit operator and the operator \hat{Q}_{se} counts the number of electrons injected in the time interval $[t_s, t_e]$, whose energy is larger than the Fermi energy E_F . By introducing the Dirac notation $\langle 1, 0; l | \psi_{[1,0]l}^c(t) \rangle = \psi_{[1,0]l}^c(t)$, the matrix element of the operator \hat{Q}_{se} can be given as

$$\langle 1, 0; l | \hat{Q}_{se} | 1, 0; l' \rangle = \int_{t_s}^{t_e} dt [\psi_{[1,0]l}^c(t)]^* \psi_{[1,0]l'}^c(t). \quad (25)$$

For a system under periodic driving, it is usually convenient to average the idle time probability over a single period:

$$\Pi(\tau) = \int_{-T/2}^{T/2} dt_s \Pi(t_s, t_s + \tau). \quad (26)$$

In doing so, one obtains the time-averaged idle time probability $\Pi(\tau)$, which only depends on the length of the time interval. The corresponding WTD can be given as

$$W(\tau) = \langle \tau \rangle \partial_\tau^2 \Pi(\tau), \quad (27)$$

with $\langle \tau \rangle$ being the mean waiting time.

The above equations offer a direct relation between the wave functions and WTD, where the overlap between levitons manifests itself as the off-diagonal elements in Eq. (25). When the overlap vanishes, the idle time probability $\Pi(t_s, t_e)$ can be reduced to

$$\Pi_c(t_s, t_e) = \prod_{l=0, \pm 1, \pm 2, \dots} \left[1 - \int_{t_s}^{t_e} dt |\psi_{[1,0]l}^c(t)|^2 \right]. \quad (28)$$

A quite similar result has been obtained for the ideal single-electron source built from the mesoscopic capacitor [63]. The corresponding WTD $W_c(\tau)$ calculated from $\Pi_c(t_s, t_e)$ can exhibit a strong peak around the point $\tau = T$ and drops rapidly to zero when $\tau > 2T$, as illustrated by the black dashed curve in Fig. 3. This indicates that one injects exactly one electron

²Note that, in this case, we have $q_{[1,0]} = 1.0$.

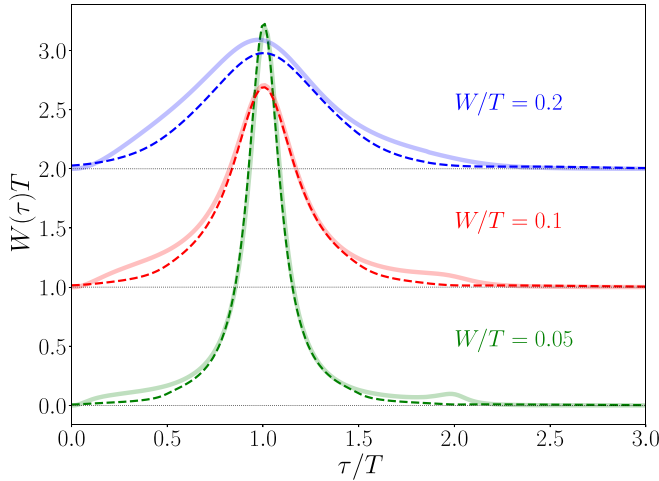


FIG. 4. The WTDs between electrons above the Fermi sea, corresponding to $Q = e$ and the width $W/T = 0.05$ (green), 0.1 (red), and 0.2 (blue). The solid curves represent the exact WTD, while the dashed curves represent the semiclassical approximation from Eq. (28). Curves corresponding to different W/T are shifted vertically for better visibility.

per period, corresponding to the case of ideal single-electron injection. In realistic conditions, Eq. (28) can be regarded as a semiclassical approximation. The presence of the overlap between levitons can lead to a deviation between the exact WTD $W(\tau)$ and the semiclassical approximation $W_c(\tau)$. This can be seen by comparing the red solid curve [$W(\tau)$] to the black dashed one [$W_c(\tau)$] in Fig. 3, which are calculated for $W/T = 0.1$. One can see that the peak in the WTD is slightly broadened due to the overlap, indicating an enhancement of the fluctuations of the waiting time.

In fact, the enhancement is not significant for $W/T = 0.1$. Moreover, it can be suppressed by decreasing W/T . This is illustrated in Fig. 4, where we compare the WTDs for the width $W/T = 0.05$, 0.1 , and 0.2 . This indicates that the ideal single-electron injection can be approached in the limit $W/T \rightarrow 0$. Accordingly, the wave functions $\psi_{[1,0]l}^c(t)$ are well separated and can be treated as individual levitons in this limit.

The above results show that levitons can be well described by the one-body wave function $\psi_{kl}^c(t)$. In the following section, we shall further demonstrate that the wave function $\psi_{kl}^c(t)$ can also be used to describe the charged quasiparticles in the fractional-charged wave packet.

IV. WAVE PACKET WITH TWO-THIRDS CHARGES

Now we turn to the wave packets carrying on average two-thirds electric charges ($Q/e = \frac{2}{3}$) per period. In this case, each wave packet still contains only one charged quasiparticle associated with the index $k = [1, 0]$. Due to the dynamical orthogonality catastrophe, one expects that the wave packet can also contain a large amount of neutral eh pairs, when the pulse width W/T is small enough. However, as it is difficult to generate well-behaved voltage pulses with too small width $W/T < 0.1$ [1,2], there exist only a rather limited number of eh pairs under typical experimental conditions. In fact,

even for the width $W/T = 0.1$, we find that the excitation probabilities p_k of the eh pairs are all smaller than 0.15 .

A. Charged quasiparticles

As a first step toward exploring the quantum state of the wave packets, let us omit the contribution of the eh pairs, which is valid for large width W/T . In doing so, the correlation function $G_{ex}(t, t')$ can be decomposed into the same form as the one of levitons [see Eq. (18)]. However, the wave function $\psi_{[1,0]l}^c(t)$ takes a different form, which can be written as

$$\psi_{[1,0]l}^c(t) = U_{[1,0]}^c(t) \frac{e^{-iq_{[1,0]}\Omega(t-IT/q_{[1,0]})/2}}{\sqrt{q_{[1,0]}}} \times \text{sinc}\left[\frac{q_{[1,0]}\Omega(t-IT/q_{[1,0]})}{2\pi}\right], \quad (29)$$

with the factor $q_{[1,0]} = \frac{2}{3}$. By comparing the wave function of levitons in Eq. (21), we show that there are two differences between the two cases: (1) the periodic function $U_{[1,0]}^c(t)$ has to be obtained numerically in this case; (2) while the function $U_{[1,0]}^c(t)$ has the period T , the sinc function in this case represents the wave packet localized around $t = l(3T/2)$. This indicates that the wave functions $\psi_{[1,0]l}^c(t)$ are characterized by two different timescales: T and $3T/2$. It is these two timescales, which makes the corresponding charged quasiparticles exhibit qualitatively different features from the ones of levitons.

The timescale $3T/2$ is directly related to the charges carried by the quasiparticles. In fact, as the wave functions $\psi_{[1,0]l}^c(t)$ with different l are still orthogonal to each other [see Eq. (15)], one can still express the current as the incoherent summation of them, which has the same form as the one of levitons [see Eq. (23)]. However, as these wave functions are separated from each other by the time interval $3T/2$, which is mismatch to the repetition period T of the pulse train (see the inset of Fig. 5), on average each quasiparticle can carry only $2e/3$ charge within a single period T . In other words, the fractional charge carried by the quasiparticle is due to the mismatch between the two timescales.

Moreover, the mismatch can also have pronounced impact on the wave functions of the quasiparticle, which can exhibit different profiles. This is also illustrated in the inset of Fig. 5. For $l = -2, 0$, and 2 (red solid curves), the wave functions $\psi_{[1,0]l}^c(t)$ can exhibit a strong peak, which is accompanied by two small shoulder peaks. In contrast, for $l = -1$ and 1 (green dashed curves), the wave functions $\psi_{[1,0]l}^c(t)$ exhibit double-peak structures. This is a direct consequence of the double periodicity of the wave functions. In fact, from Eq. (29), one can see that when the timescale corresponding to $U_{[1,0]}^c(t)$ (T) and the sinc function ($T/q_{[1,0]}$) do not match, for $q_{[1,0]} = A/B$ (with A and B being coprime integers), the wave functions can exhibit A different profiles, which are separated from each other with the extended period BT/A .

Due to the mismatch between the two periods, the wave functions are strongly overlapping with each other. This can be seen intuitively from the inset of Fig. 5. The overlap can induce a large fluctuation of the waiting time, which can be

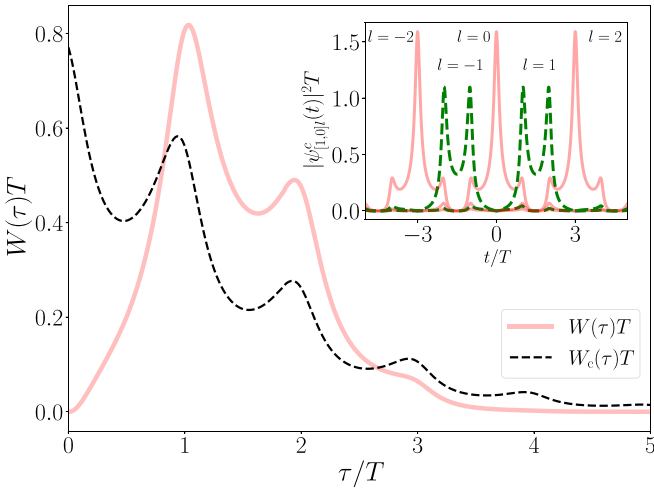


FIG. 5. The WTD between electrons above the Fermi sea, corresponding to the width $W/T = 0.1$. The corresponding train of charged quasiparticles is illustrated by the wave functions $|\psi_{[1,0]l}^c(t)|^2 T$ in the inset. The red solid curves correspond to $l = -2, 0, \text{ and } 2$, while the green dashed curves correspond to $l = -1$ and 1 .

seen from the corresponding WTD.³ This is illustrated by the red solid curves in the main panel of Fig. 5. One can see that the WTD exhibits a series of peaks at multiples of the repetition period T . This indicates the presence of the cycle-missing event, in which the voltage pulse can fail to inject an electron within a single period T [63,64].

As the overlap between the wave functions are rather large, the semiclassical approximation $W_c(\tau)$ of the WTD [Eq. (28)] is inapplicable. One can see that $W_c(\tau)$ largely overestimates the WTD around the point $\tau = 0$, which is illustrated by the black dashed curve in Fig. 5. In fact, $W_c(\tau)$ gives an unphysical value around this point: The WTD should be zero at $\tau = 0$ due to the Pauli principle. Unlike the case of levitons, the overlap between the wave functions cannot be eliminated by just decreasing the width W/T . As a consequence, the multiple-peak structure of the WTD is preserved as W/T decreases. This is illustrated in Fig. 6, corresponding to $W/T = 0.2, 0.1$, and 0.05 .

The above results explain the nature of the charged quasiparticles in the wave packet carrying fractional charges per period: they are just quasiparticles injected with an extended period T/q_k , which is longer than the period T of the driving pulses. The wave functions of these quasiparticles are always strongly overlapping with each other, manifesting themselves at multiple peaks in the corresponding WTD. The feature of these quasiparticles can be characterized by the factor q_k , indicating that each quasiparticle can carry eq_k charges per period T , making them behave *effectively* as fractional-charged quasiparticles.

³Generally speaking, the electron component of the eh pairs can also contribute to the WTD. However, the contribution remains negligible due to the small excitation probability for the width $W/T > 0.05$.

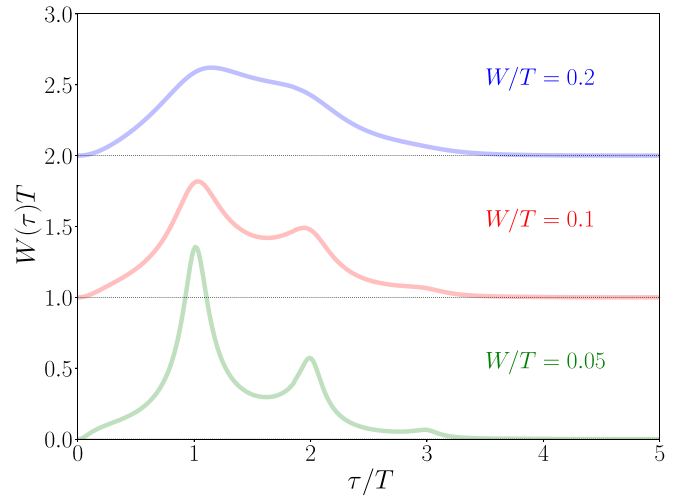


FIG. 6. The WTD between electrons above the Fermi sea, corresponding to $Q/e = \frac{2}{3}$ and the width $W/T = 0.05$ (green), 0.1 (red), and 0.2 (blue). Curves corresponding to different W/T are shifted vertically for better visibility.

B. Electron-hole pairs

Now let us briefly discuss the eh pairs in the wave packet. For $W/T = 0.1$, we find that each wave packet contains only one eh pair, which is associated with the index $k = [0, 0]$. The corresponding excitation probability $p_{[0,0]}$ is only 0.138 . The other eh pairs are negligible due to their small excitation probabilities.⁴ The eh pairs can be described in a similar way as the charged quasiparticles. In fact, the wave functions of the electron and hole components can be expressed in the same form as shown in Eq. (29):

$$\psi_{[0,0]l}^{e/h}(t) = U_{[0,0]}^{e/h}(t) \frac{e^{-iq_{[0,0]}\Omega(t-lT/q_{[0,0]})/2}}{\sqrt{q_{[0,0]}}} \times \text{sinc}\left[\frac{q_{[0,0]}\Omega(t-lT/q_{[0,0]})}{2\pi}\right] \quad (30)$$

with the factor $q_{[0,0]} = \frac{1}{3}$. The corresponding wave functions $\psi_{[1,0]l}^{e/h}(t)$ are plotted by the green and blue curves in Fig. 7, where the wave functions $\psi_{[1,0]l}^c(t)$ of the charged quasiparticles are also plotted by the red curves for comparison. One can see that in this case, the wave functions for the electron (hole) component exhibit only one type of profile. They are separated from each other by the time interval $3T$, making them behave as quasiparticles carrying $e/3$ charges. Note that electron and hole components carry the same amount of charges but with opposite sign, which cannot contribute to the total charge Q of the wave packet.

By combining the information of both the charged quasiparticles and eh pairs, the quantum state of the whole train of

⁴They are all smaller than 0.002 .

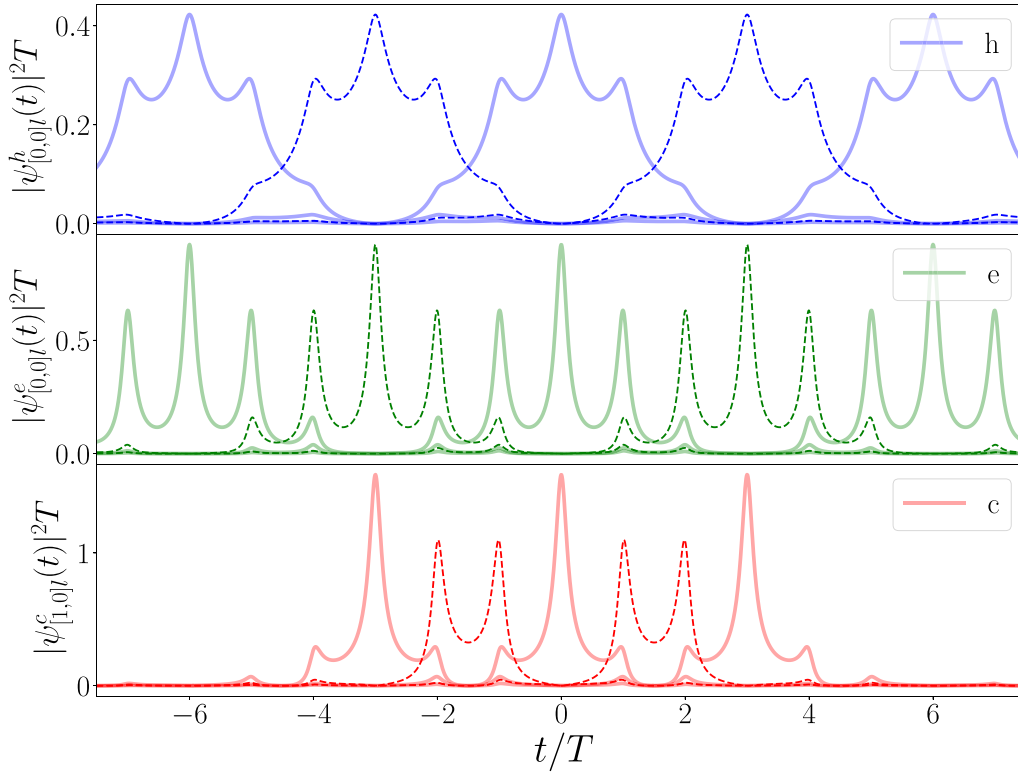


FIG. 7. Wave functions of the charged quasiparticle ($k = [1, 0]$) and the eh pair ($k = [0, 0]$). The red curves represent the wave functions of the charged quasiparticle. The green and blue curves represent the wave functions for the electron and hole components of the eh pair, respectively. All the wave functions are calculated with $W/T = 0.1$. The solid (dashed) curves from left to right correspond to $l = -2, 0$, and 2 ($l = -1$ and 1), respectively.

wave packet can be written as

$$|\Psi_{\text{train}}\rangle = \prod_{l=0,\pm 1,\pm 2,\dots} C_{[1,0]l}^\dagger [\sqrt{1-p_{[0,0]}} + i\sqrt{p_{[0,0]}}(B_{[0,0]l}^e)^\dagger (B_{[0,0]l}^h)^\dagger] |\mathbf{F}\rangle, \quad (31)$$

with

$$\begin{aligned} C_{[1,0]l}^\dagger &= \int_{-\infty}^{+\infty} dt \psi_{[1,0]l}^c(t) \hat{a}^\dagger(t), \\ (B_{[0,0]l}^e)^\dagger &= \int_{-\infty}^{+\infty} dt \psi_{[0,0]l}^e(t) \hat{a}^\dagger(t), \\ (B_{[0,0]l}^h)^\dagger &= \int_{-\infty}^{+\infty} dt \psi_{[0,0]l}^h(t) \hat{a}^\dagger(t). \end{aligned} \quad (32)$$

This provides a full information of the injected electric wave packet. It allows us to elucidate how the quantum state of wave packets can evolve as the flux of the pulses changes. In the following section, we shall concentrate on the evolution of the charged quasiparticles. We shall show how levitons can emerge as the flux approaches an integer value.

V. EVOLUTION OF CHARGED QUASIPARTICLE

The evolution of the charged quasiparticles can be fully described by the one-body wave function $\psi_{kl}^c(t)$. This is illustrated in Fig. 8, corresponding to the index $k = [1, 0]$.

In the figure, we choose $W/T = 0.1$ and $Q/e \in (0.0, 2.0)$. Curves with different colors and line types correspond to wave functions $\psi_{[1,0]l}^c(t)$ with different l . As the factor $q_{[1,0]}$ can play an important role, we also show the corresponding $q_{[1,0]}$ alongside the wave functions.

From the figure, one first notices that one has $q_{[1,0]} = Q/e$ when $Q/e \in (0.0, 1.0)$. For $q_{[1,0]} = \frac{1}{4}$, all the wave functions of the quasiparticles exhibit the same profile. These quasiparticles are injected with the extended period $4T$, indicating that they can carry $e/4$ charge within each period T . As $q_{[1,0]}$ increases from $\frac{1}{4}$ to $\frac{1}{2}$, the extended period is reduced to $2T$, indicating that the quasiparticles evolve into the $e/2$ -charged quasiparticles. As $q_{[1,0]}$ further increases from $\frac{1}{2}$ to $\frac{3}{4}$, there can exist three types of quasiparticle, which are injected with the extended period $3T/4$, leading to $3e/4$ charges per period. As $q_{[1,0]}$ reaches 1.0, all the quasiparticles can evolve into levitons, which are injected with the period T .

For $Q/e \in (1.0, 2.0)$, one has $q_{[1,0]} = 2 - Q/e$. As Q/e increases in this region, $q_{[1,0]}$ drops linearly to zero. Accordingly, the levitons can evolve back into fractionally charged quasiparticles, which are injected with the extended period $T/q_{[1,0]}$. Note that one has $T/q_{[1,0]} \rightarrow +\infty$ for $q_{[1,0]} \rightarrow 0$. This implies that the corresponding quasiparticles cannot be injected in this limit since the time interval between successive quasiparticle injection tends to infinity. From Eq. (16), one can see that the factor $q_{[n,m]}$ can take nonzero value when $Q/e \in [n-1, n+1]$. This indicates that the corresponding quasiparticle can only be injected inside this region.

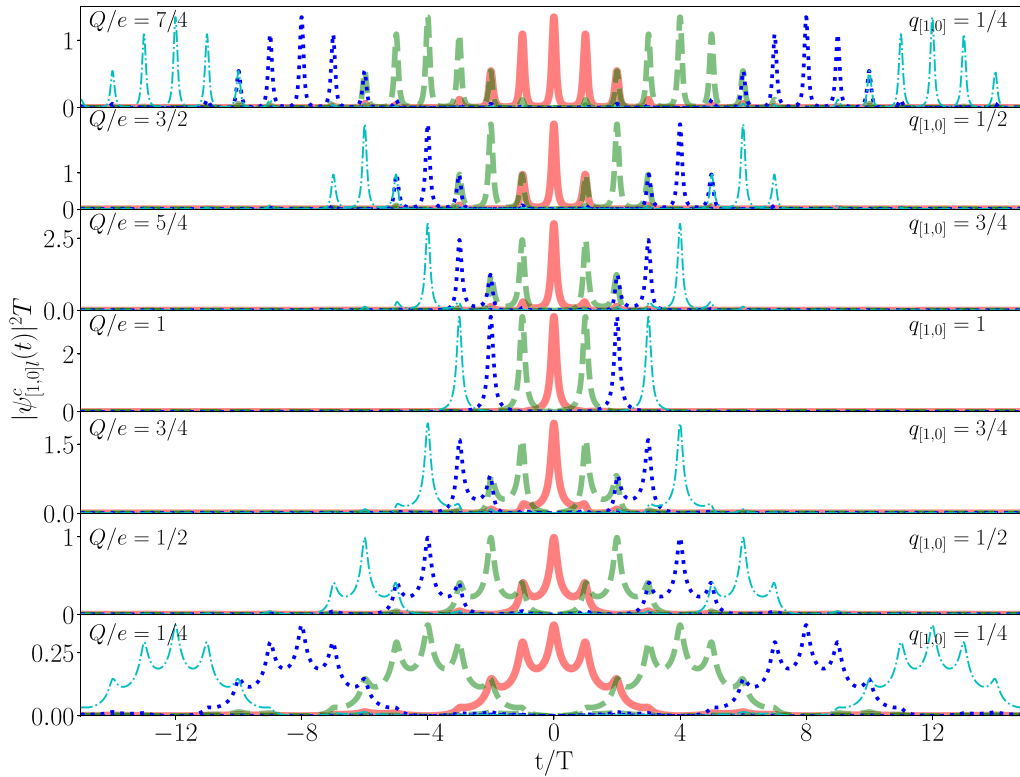


FIG. 8. Wave functions of the charged quasiparticle $|\psi_{[1,0]l}^c(t)|^2 T$, corresponding to $W/T = 0.1$ and $Q/e \in (0.0, 2.0)$. For each value of Q/e , we plot the wave functions for $l = -3 \sim 3$. Curves with different colors and line types correspond to $|\psi_{[1,0]l}^c(t)|^2 T$ with different l .

The available quasiparticles for a given Q/e can then be illustrated intuitively by using the factor $q_{[n,m]}$, which is shown in Fig. 9.

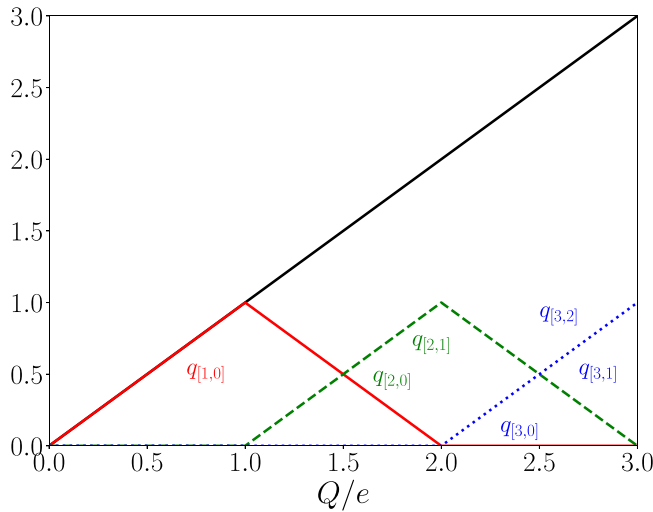


FIG. 9. Factor q_k as functions of Q/e . The red solid curve represents $q_{[1,0]}$. The green dashed curves represent $q_{[2,0]}$ and $q_{[2,1]}$. Note that one has $q_{[2,0]} = q_{[2,1]}$, so the two curves are overlapped. Similarly, the blue-dotted curves represent $q_{[3,0]}$, $q_{[3,1]}$, and $q_{[3,2]}$, which satisfies $q_{[3,0]} = q_{[3,1]} = q_{[3,2]}$. The black solid curve represents the charge of the wave packet Q/e , which satisfies $Q = e \sum_k q_k$.

The evolution of the quasiparticles can also be seen from the corresponding WTD, as illustrated in Fig. 10. One can see that for $Q/e = \frac{1}{4}$, the waiting time has a rather wide distribution. This is because the corresponding wave functions of the quasiparticles are strongly overlapping, as shown in Fig. 8. As Q/e approaches 1.0, the WTD $W(\tau)$ tends to exhibit a strong peak around $\tau = T$, indicating the emergence of

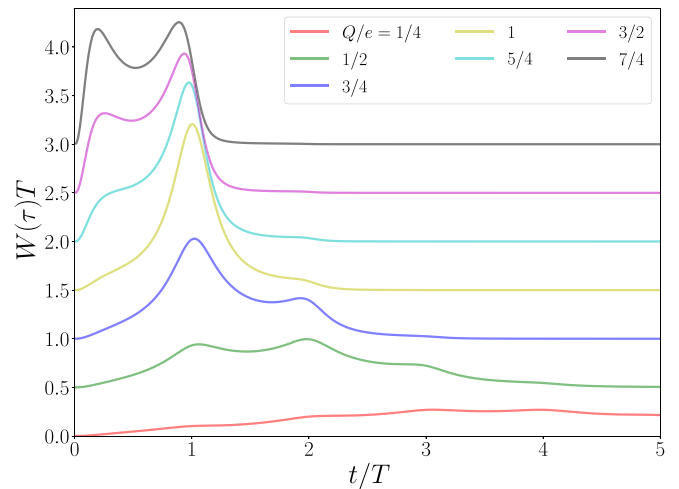


FIG. 10. The WTDs between electrons above the Fermi sea, corresponding to $Q/e \in (0.0, 2.0)$ and the width $W/T = 0.1$. Curves corresponding to different Q/e are shifted vertically for better visibility.

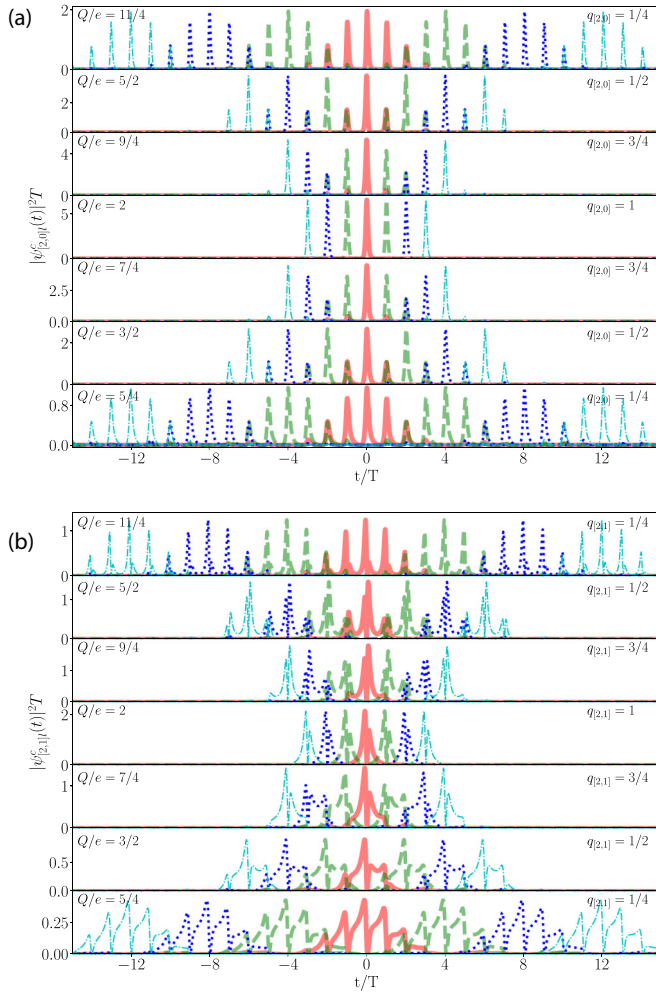


FIG. 11. Wave functions of the charged quasiparticle $|\psi_{[2,0]}^c(t)|^2 T$ (a) and $|\psi_{[2,1]}^c(t)|^2 T$ (b), corresponding to $W/T = 0.1$ and $Q/e \in (1.0, 3.0)$. For each value of Q/e , we plot the wave functions for $l = -3 \sim 3$. Curves with different colors and line types correspond to the wave functions with different l .

levitons. Hence the evolution of the wave functions for $Q/e < 1.0$ can also be tracked by using the corresponding WTD. As Q/e goes above 1.0, additional charged quasiparticles can be injected. From Fig. 9, one can see that two additional quasiparticles $k = [2, 0]$ and $[2, 1]$ can emerge. The evolution of these two quasiparticles is demonstrated in Fig. 11. By comparing to Fig. 8, one can see that they evolve in a similar way as the quasiparticle $k = [1, 0]$. As these two quasiparticles can also contribute to the WTD, it is difficult to read the evolution of a single charged quasiparticles from the WTD when $Q/e > 1.0$.

VI. EVOLUTION OF ELECTRON-HOLE PAIRS AND SHOT NOISE

As levitons evolve into charged quasiparticles carrying effectively fractional charges, additional eh pairs can be excited. Due to the small excitation probabilities, the eh pairs can have little contribution to the WTD between electrons above the

Fermi sea.⁵ In contrast, it can have pronounced impact on the shot noise, which has been extensively studied in previous works [2,32,33,41]. When the wave packet is partitioned at a localized scatter with transmission probability D , both the charged quasiparticles and eh pairs can contribute to the shot noise S_N . It can be decomposed into two parts (see Appendix B for details): $S_N = S_c + S_{ex}$, where

$$S_c = S_0 \sum_k q_k,$$

$$S_{ex} = 2S_0 \sum_k q_k p_k. \quad (33)$$

with $S_0 = 2 \frac{e^2}{h} D(1-D) \hbar \Omega$ being the typical scale of the shot noise.

The first part corresponds to the contribution of the charged quasiparticles. It is solely decided by the charge Q of the wave packet since one has $\sum_k q_k = Q/e$ from Eq. (16). The second part is the excess shot noise, which has been used extensively to characterize the feature of eh pairs [2,65]. By using the information of the excitation probability p_k and the factor q_k , one can decompose the excess shot noise S_{ex} into the contribution of individual eh pairs. This is illustrated in Fig. 12. From the figure, one can identify the contribution of three eh pairs, corresponding to $k = [0, 0]$, $[1, 1]$, and $[2, 2]$. These eh pairs dominate the excess shot noise S_{ex} in different regions. Such decomposition makes it possible to extract the information of individual eh pairs from the excess shot noise. By combining the WTD with the shot noise, one can hence obtain the full information of the evolution of the quantum state of the wave packet.

VII. SUMMARY AND OUTLOOK

In summary, we have presented a general approach to extract the quantum state of wave packets injected by Lorentzian pulse train with arbitrary flux. We show that the charged quasiparticles can be described by a set of one-body wave functions $\psi_{kl}^c(t)$. These wave functions can be regarded as Martin-Landauer-type wave packets, which offer an intuitive way to interpret their time-resolved behaviors. In integer-charged wave packets, the charged quasiparticles are levitons, which are injected with the same period as the pulse train. No eh pairs can be injected in this case. In fractional-charged wave packets, the injection of the charged quasiparticles is characterized by two different timescales, which are decided by the repetition period T of the pulse train and T rescaled by a factor related to the flux φ of the pulse. Due to the mismatch between the two different timescales, the wave functions of the quasiparticles can exhibit different profiles. They can form a periodic train, whose period is longer than the repetition period T of the pulse train. This makes them behave effectively as quasiparticles carrying fractional charges. By using the wave function of the charged quasiparticles, we demonstrate how levitons can evolve as the flux φ of pulse changes.

⁵Generally speaking, the electron component of the eh pair can also contribute to the WTD between electrons above the Fermi sea. However, the contribution remains negligible for $W/T = 0.05$.

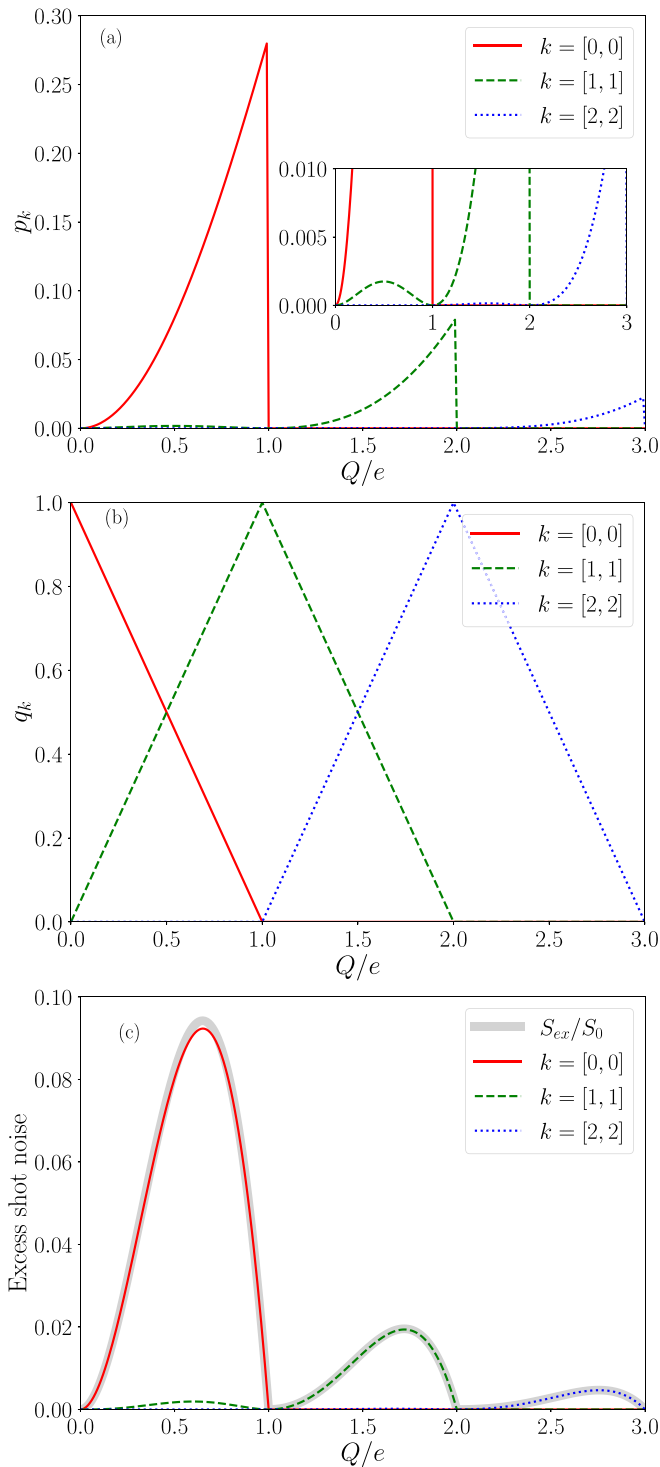


FIG. 12. (a) The excitation probabilities p_k for the eh pairs. The inset shows the zoom-in of the figure. The p_k of other eh pairs are too small to be seen from the figure. (b) The injection probabilities q_k of the electron and hole components of the eh pairs. (c) Excess shot noise S_{ex} as a function of the charge Q/e of the wave packet. The red solid, green dashed, and blue dotted curves represent the contribution from the eh pairs $k = [0, 0]$, $[1, 1]$, and $[2, 2]$, respectively. The excess shot noise is normalized to $S_0 = 2\frac{e^2}{h}D(1 - D)\hbar\Omega$.

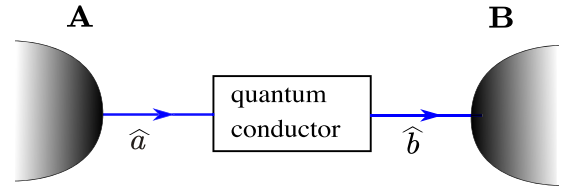


FIG. 13. A single-channel quantum conductor connected to two reservoirs **A** and **B**.

We also show that such evolution can be seen from the WTD between electrons above the Fermi sea. Our approach can also be used to describe the evolution of eh pairs, which can be tracked by using the shot noise. Note that although our approach is demonstrated for the Lorentzian pulses, it is rather general and can be applied to pulses with arbitrary profiles. We expect our work will be helpful to explore the full potential of the voltage electron source.

ACKNOWLEDGMENTS

The authors would like to thank Prof. D. C. Glattli and Prof. M. V. Moskalets for helpful comments and discussion. We wish to thank the anonymous referees for the careful reading of the manuscript, constructive suggestions, and helpful feedback. The suggestions on the Martin-Landauer wave packet and idle time probability are particularly valuable for this work. This work was supported by the Key Program of National Natural Science Foundation of China under Grant No. 11234009, Young Scientists Fund of National Natural Science Foundation of China under Grant No. 11504248, and the Fostering Program in Disciplines Possessing Novel Features for Natural Science of Sichuan University under Grant No. 2020SCUNL209.

APPENDIX A: BLOCH-MESSIAH REDUCTION WITHIN THE FRAMEWORK OF SCATTERING MATRIX THEORY

The basic idea is straightforward: In a noninteracting electron system, the many-body state can be expressed as a Slater determinant in the zero-temperature limit, which can be fully determined by the one-body correlation function [53,66]. By calculating the correlation function based on the scattering matrix theory of quantum transport, one can reconstruct the Slater determinant from the scattering matrix.

Such reconstruction can be demonstrated more clearly in a single-channel quantum conductor at zero temperature, as illustrated in Fig. 13. The incoming electrons are injected from the reservoir **A** into the conductor, while the outgoing electrons from the conductor are fed into the reservoir **B**. Without interactions, the quantum transport of electrons in such system can be generally described by a one-body scattering matrix \mathbf{S} . By introducing annihilation operators $\hat{a}(E)$ and $\hat{b}(E)$ for the incoming and outgoing electrons in the energy domain, one has

$$\hat{b}(E) = \sum_{E'} \mathbf{S}(E, E') \hat{a}(E'), \quad (\text{A1})$$

with $\mathbf{S}(E, E')$ representing the matrix element of the scattering matrix \mathbf{S} in the energy domain.

It is convenient to introduce the polar decomposition of the scattering matrix, which has the form

$$\mathbf{S}(E, E') = \sum_j [\psi_j^e(E), \psi_j^h(E')] \times \begin{bmatrix} \sqrt{1-p_j} & i\sqrt{p_j} \\ i\sqrt{p_j} & \sqrt{1-p_j} \end{bmatrix} \begin{bmatrix} \varphi_j^e(E') \\ \varphi_j^h(E') \end{bmatrix}^*, \quad (\text{A2})$$

where $\psi_j^e(E)$, $\varphi_j^e(E')$ are nonzero for $E > 0$, while $\psi_j^h(E)$, $\varphi_j^h(E')$ are nonzero for $E \leq 0$. These functions form orthonormal basis in the energy domain:

$$\int \frac{dE}{2\pi\hbar} \langle \alpha'_j | E \rangle \langle E | \alpha_j \rangle = \delta_{j,j'} \delta_{\alpha,\alpha'}, \quad (\text{A3})$$

with $\delta_{j,j'}$ being the Kronecker delta. Note that we have introduced the Dirac notation $\langle E | \alpha_k \rangle = \psi_j^\alpha(E)$, with $\alpha = e, h$.

Now let us turn to discuss the many-body state of the electrons in such system. For the incoming electrons, the many-body state $|\Psi_{\mathbf{A}}\rangle$ is just a Fermi sea $|\mathbf{F}\rangle$, whose Fermi level E_F is decided by the reservoir \mathbf{A} . Assuming $E_F = 0$, it can be expressed as

$$|\Psi_{\mathbf{A}}\rangle = |\mathbf{F}\rangle = \prod_{\epsilon \leq 0} \hat{a}^\dagger(\epsilon) |\mathbf{Vac}\rangle, \quad (\text{A4})$$

with $|\mathbf{Vac}\rangle$ being the vacuum state.

Alternatively, one can also describe the many-body state $|\Psi_{\mathbf{A}}\rangle$ by using the corresponding one-body correlation function, which has the form in the energy domain

$$iG_{\mathbf{A}}^<(E, E') = \langle \mathbf{F} | \hat{a}^\dagger(E') \hat{a}(E) | \mathbf{F} \rangle \quad (\text{A5})$$

or, equivalently,

$$iG_{\mathbf{A}}^>(E, E') = \langle \mathbf{F} | \hat{a}(E) \hat{a}^\dagger(E') | \mathbf{F} \rangle, \quad (\text{A6})$$

which related to $G_{\mathbf{A}}^<(E, E')$ as $G_{\mathbf{A}}^<(E, E') + G_{\mathbf{A}}^>(E, E') = i\delta(E - E')$.

By substituting Eq. (A4) into Eqs. (A5) and (A6), the correlation function $G_{\mathbf{A}}^>$ can be expressed by using the one-body states $|\epsilon\rangle$ of electrons as

$$iG_{\mathbf{A}}^<(E, E') = \sum_{\epsilon \leq 0} \langle E | \epsilon \rangle \langle \epsilon | E' \rangle, \quad (\text{A7})$$

$$iG_{\mathbf{A}}^>(E, E') = \sum_{\epsilon > 0} \langle E | \epsilon \rangle \langle \epsilon | E' \rangle,$$

with $\langle E | \epsilon \rangle = \delta(E - \epsilon) \Delta E$. Here ΔE is the mesh size in the energy domain. The limit $\Delta E \rightarrow 0$ should be taken in the end of the calculation.

The many-body state $|\Psi_{\mathbf{B}}\rangle$ of the outgoing electrons is usually not given explicitly in the scattering matrix theory. Instead, it is described by the one-body correlation function as

$$G_{\mathbf{B}}^<(E, E') = \langle \mathbf{F} | \hat{b}^\dagger(E') \hat{b}(E) | \mathbf{F} \rangle = \sum_{E_1, E_1'} \langle \mathbf{F} | [\mathbf{S}(E', E_1')]^* \mathbf{S}(E, E_1) \hat{a}^\dagger(E_1') \hat{a}(E_1) | \mathbf{F} \rangle. \quad (\text{A8})$$

To find the explicit form of the many-body state $|\Psi_{\mathbf{B}}\rangle$, we write $G_{\mathbf{B}}^>(E, E')$ in a form analogous to Eqs. (A7). This can be done by using the polar decomposition of the scattering matrix given in Eq. (A2), which gives

$$G_{\mathbf{B}}^>(E, E') = \sum_j \langle E | \gamma_j^> \rangle \langle \gamma_j^> | E' \rangle, \quad (\text{A9})$$

with

$$\begin{aligned} |\gamma_j^< \rangle &= i\sqrt{p_j} |e_j\rangle + \sqrt{1-p_j} |h_j\rangle, \\ |\gamma_j^> \rangle &= i\sqrt{p_j} |h_j\rangle + \sqrt{1-p_j} |e_j\rangle. \end{aligned} \quad (\text{A10})$$

This indicates that the many-body state $|\Psi_{\mathbf{B}}\rangle$ can be expressed in a BCS-like form, corresponding to a neutral cloud of eh pairs. The quantum state of the eh pair can be described by the excitation probability p_k and the one-body state $|e_k\rangle$ ($|h_k\rangle$) of the electron (hole) components. They can be obtained by solving the polar decomposition of the scattering matrix. In our previous works [54,55], we have studied the quantum state of eh pairs by using such decomposition.

It is possible for the polar decomposition to give solutions corresponding to either $|e_j\rangle = 0$ or $|h_j\rangle = 0$, when $p_j = 1.0$. This indicates that there also exist unpaired electrons or holes, which are just quasiparticles carrying negative or positive charges. Moreover, additional normalization factors can also emerge, representing the injection probability of the corresponding quasiparticles. This is the case we have encountered in this paper, when the corresponding one-body correlation function can be given as

$$G_{\mathbf{B}}^>(E, E') = \sum_j q_j \langle E | \gamma_j^> \rangle \langle \gamma_j^> | E' \rangle. \quad (\text{A11})$$

By taking these ingredients into consideration, one can express the many-body state as given in Eqs. (1)–(3). The correlation function in the time domain can be obtained from the transform

$$G^>(t, t') = \int \frac{dE dE'}{(2\pi\hbar)^2} e^{-iEt/\hbar + iE't'/\hbar} G^>(E, E'). \quad (\text{A12})$$

Note that in the main text, we have expressed the one-body correlation function $G_{\mathbf{B}}^<(t, t') = G(t, t')$ in the time domain [see Eq. (17)].

For the system we considered here, the scattering matrix has a simple structure in the time domain [see Eq. (5)]. By introducing the wave-packet functions

$$\varphi_{kl}^{e/h}(t) = \int \frac{dE}{2\pi\hbar\sqrt{q_k}} e^{-iE(t-T/q_k)/\hbar} \varphi_k^{e/h}(E), \quad (\text{A13})$$

$$\psi_{kl}^{e/h}(t) = \int \frac{dE}{2\pi\hbar\sqrt{q_k}} e^{-iE(t-T/q_k)/\hbar} \psi_k^{e/h}(E),$$

with q_k being the normalization factor, the polar decomposition [Eq. (A2)] can be obtained by solving the equations

$$e^{-i\phi(t)} \begin{bmatrix} \varphi_{kl}^e(t) \\ \varphi_{kl}^h(t) \end{bmatrix} = \sqrt{1-p_k} \begin{bmatrix} \psi_{kl}^e(t) \\ \psi_{kl}^h(t) \end{bmatrix} + i\sqrt{p_k} \begin{bmatrix} \psi_{kl}^h(t) \\ \psi_{kl}^e(t) \end{bmatrix}, \quad (\text{A14})$$

where we have chosen the compound index $j = [k, l]$. Here $\phi(t)$ is the forward scattering phase, which can be written as $\phi(t) = \frac{e}{\hbar} \int^t V(\tau) d\tau$.

Although $V(t)$ is periodic, the forward scattering phase $\phi(t)$ is nonperiodic. In fact, it is possible to extract the periodic part from $\phi(t)$ by introducing the relation

$$\varphi = N_T + \frac{\omega_T}{\Omega}, \quad (\text{A15})$$

with N_T being integer and ω_T being real number, which satisfies $\omega_T \in [0, \Omega]$. By using N_T and ω_T , one can express $\phi(t)$ as

$$\phi(t) = \phi_n(t) + [\omega_T + (N_T - n)\Omega]t, \quad (\text{A16})$$

where $\phi_n(t)$ represents the periodic part of the forward scattering phase, with n being integer.

Hence, the integer n offers a natural index for the solutions. For a given n , Eqs. (A13) and (A14) can be reduced to a singular value problem, whose solutions can be labeled by another integer m . That is why we choose the index $k = [n, m]$ in the main text. Note that for a given flux $\varphi = Q/e$, we find that only the solutions related to $n = N_T$ and $N_T - 1$ are relevant. The corresponding $\psi_k^{e/h}(t)$ can be expressed by the ansatz

$$\psi_{kl}^{e/h}(t) = U_k^{e/h}(t) \int \frac{d\omega}{2\pi\sqrt{q_k}} F_k^Q(\omega) e^{-i\omega(t-T/q_k)}, \quad (\text{A17})$$

where $F_k^Q(\omega)$ is the real function given in Eq. (13). The function $U_k^{e/h}(t)$ is periodic in the time domain, which usually has to be obtained numerically from the singular value problem.

APPENDIX B: CURRENT AND SHOT NOISE

Various observable quantities can be calculated directly from the expression of the many-body state $|\Psi_B\rangle$ given in Appendix A. The current carried by the train of wave packets can be given as

$$\begin{aligned} I(t) &= e \langle \Psi_{\text{train}} | \hat{a}^\dagger(t) \hat{a}(t) | \Psi_{\text{train}} \rangle \\ &= \sum_k \sum_{l=0, \pm 1, \pm 2, \dots} I_{kl}^c(t) + \sum_k \sum_{l=0, \pm 1, \pm 2, \dots} I_{kl}^{eh}(t), \end{aligned} \quad (\text{B1})$$

where $I_k^c(t)$ represents the contribution from the charged quasiparticles, which has the form

$$I_{kl}^c(t) = eq_k |\psi_{kl}^c(t)|^2. \quad (\text{B2})$$

In contrast, $I_{kl}^{eh}(t)$ represents the contribution from the eh pair, which can be written as

$$\begin{aligned} I_{kl}^{eh}(t) &= eq_k p_k [|\psi_{kl}^e(t)|^2 - |\psi_{kl}^h(t)|^2] \\ &\quad + 2eq_k \sqrt{p_k(1-p_k)} \text{Im} \{ \psi_{kl}^h(t) [\psi_{kl}^e(t)]^\dagger \}. \end{aligned} \quad (\text{B3})$$

Note that for the electron source we considered here, one always has $I(t) = (e^2/h)V(t)$.

When the train of wave packets is partitioned at a localized scatter with transmission probability D , both the quasiparticles and eh pairs can contribute to the shot noise. The time-dependent shot noise can be expressed as

$$S_{sn}(t, t') = e^2 D(1-D) \frac{i}{2\pi} \frac{1}{t - t' + i\eta}$$

$$\begin{aligned} &\times \sum_k q_k \sum_{l=0, \pm 1, \pm 2, \dots} \{ \psi_{kl}^c(t) [\psi_{kl}^c(t')]^\dagger \\ &\quad + [\sqrt{p_k} \psi_{kl}^e(t) - i\sqrt{1-p_k} \psi_{kl}^h(t)] \\ &\quad \times [\sqrt{p_k} \psi_{kl}^e(t') - i\sqrt{1-p_k} \psi_{kl}^h(t')]^\dagger \\ &\quad + [\sqrt{p_k} \psi_{kl}^h(t') - i\sqrt{1-p_k} \psi_{kl}^e(t') \\ &\quad \times [\sqrt{p_k} \psi_{kl}^h(t) - i\sqrt{1-p_k} \psi_{kl}^e(t)]^\dagger \}. \end{aligned} \quad (\text{B4})$$

The shot noise in the dc limit can be obtained as

$$\begin{aligned} \overline{S_{sn}(t, t')} &= \int_{-\infty}^{+\infty} \int_{-\infty}^{+\infty} S_{sn}(t, t') dt dt' \\ &= \sum_{l=0, \pm 1, \pm 2, \dots} [S_c(l) + S_{ex}(l)], \end{aligned} \quad (\text{B5})$$

where $S_c(l)$ and $S_{ex}(l)$ representing the shot noise attributed to the charged quasiparticles and eh pairs in the l th wave packet. We find that both of them are independent on the index l , which can be written as

$$\begin{aligned} S_c &= S_0 \sum_k q_k, \\ S_{ex} &= 2S_0 \sum_k q_k p_k \end{aligned} \quad (\text{B6})$$

with $S_0 = 2\frac{e^2}{h}D(1-D)\hbar\Omega$ being the typical scale of the shot noise.

APPENDIX C: WAITING TIME DISTRIBUTION

To obtain the information of the many-body state in short timescales, we study the waiting time distribution between electrons above the Fermi sea. This can be obtained from the idle time probability [51,62,63,67]. Given a time interval $[t_s, t_e]$, the corresponding idle time probability $\Pi(t_s, t_e)$ can be given as

$$\Pi(t_s, t_e) = \langle \Psi_B | : e^{i\hat{N}_{se}} : | \Psi_B \rangle, \quad (\text{C1})$$

where $: \dots :$ represents the normal ordering. The operator \hat{N}_{se} counts the number of electrons above the Fermi sea injected in the given time interval, which can be given as

$$\hat{N}_{se} = \int_{t_s}^{t_e} dt \hat{a}_p^\dagger(t) \hat{a}_p(t), \quad (\text{C2})$$

with $\hat{a}_p(t) = \int_0^{+\infty} e^{-iEt/\hbar} \hat{a}(E) dE / (2\pi\hbar)$.

It is convenient to calculate idle time probability by using the decomposition introduced in Appendix A. By introducing the operator corresponding to the one-body correlation function $\hat{G}_B^< = \sum_j q_j |\gamma_j^<\rangle \langle \gamma_j^<|$, we find

$$\Pi(t_s, t_e) = \det[\hat{1} - \hat{\Lambda}_{se} \hat{G}_B^<], \quad (\text{C3})$$

where we have introduced a one-body operator $\hat{\Lambda}_{se} = \int_{t_s}^{t_e} dt |t_p\rangle \langle t_p|$ corresponding to \hat{N}_{se} , with $|t_p\rangle = \int_0^{+\infty} e^{iEt/\hbar} |E\rangle dE / (2\pi\hbar)$. Equation (24) can be obtained by defining $\hat{Q}_{se} = \hat{\Lambda}_{se} \hat{G}_B^<$ in Eq. (C3).

- [1] J. Dubois, T. Jullien, F. Portier, P. Roche, A. Cavanna, Y. Jin, W. Wegscheider, P. Roulleau, and D. C. Glatli, *Nature (London)* **502**, 659 (2013).
- [2] J. Dubois, T. Jullien, C. Grenier, P. Degiovanni, P. Roulleau, and D. C. Glatli, *Phys. Rev. B* **88**, 085301 (2013).
- [3] J. Keeling, I. Klich, and L. S. Levitov, *Phys. Rev. Lett.* **97**, 116403 (2006).
- [4] E. Bocquillon, V. Freulon, J.-M. Berroir, P. Degiovanni, B. Plaçais, A. Cavanna, Y. Jin, and G. Fève, *Science* **339**, 1054 (2013).
- [5] P. P. Hofer and M. Büttiker, *Phys. Rev. B* **88**, 241308(R) (2013).
- [6] M. Moskalets, G. Haack, and M. Büttiker, *Phys. Rev. B* **87**, 125429 (2013).
- [7] J. Gabelli and B. Reulet, *Phys. Rev. B* **87**, 075403 (2013).
- [8] T. Jullien, P. Roulleau, B. Roche, A. Cavanna, Y. Jin, and D. C. Glatli, *Nature (London)* **514**, 603 (2014).
- [9] G. Fève, A. Mahé, J. M. Berroir, T. Kontos, B. Plaçais, D. C. Glatli, A. Cavanna, B. Etienne, and Y. Jin, *Science* **316**, 1169 (2007).
- [10] J. Keeling, A. V. Shytov, and L. S. Levitov, *Phys. Rev. Lett.* **101**, 196404 (2008).
- [11] A. Mahé, F. D. Parmentier, E. Bocquillon, J.-M. Berroir, D. C. Glatli, T. Kontos, B. Plaçais, G. Fève, A. Cavanna, and Y. Jin, *Phys. Rev. B* **82**, 201309(R) (2010).
- [12] M. Albert, C. Flindt, and M. Büttiker, *Phys. Rev. B* **82**, 041407(R) (2010).
- [13] Y. Sherkunov, N. d'Ambrumenil, P. Samuelsson, and M. Büttiker, *Phys. Rev. B* **85**, 081108(R) (2012).
- [14] E. Bocquillon, F. D. Parmentier, C. Grenier, J.-M. Berroir, P. Degiovanni, D. C. Glatli, B. Plaçais, A. Cavanna, Y. Jin, and G. Fève, *Phys. Rev. Lett.* **108**, 196803 (2012).
- [15] J. D. Fletcher, P. See, H. Howe, M. Pepper, S. P. Giblin, J. P. Griffiths, G. A. C. Jones, I. Farrer, D. A. Ritchie, T. J. B. M. Janssen, and M. Kataoka, *Phys. Rev. Lett.* **111**, 216807 (2013).
- [16] N. Ubbelohde, F. Hohls, V. Kashcheyevs, T. Wagner, L. Fricke, B. Kästner, K. Pierz, H. W. Schumacher, and R. J. Haug, *Nat. Nanotechnol.* **10**, 46 (2014).
- [17] S. Ryu, M. Kataoka, and H.-S. Sim, *Phys. Rev. Lett.* **117**, 146802 (2016).
- [18] J. Splettstoesser and R. J. Haug, *Phys. Status Solidi B* **254**, 1770217 (2017).
- [19] M. Misiorny, G. Fève, and J. Splettstoesser, *Phys. Rev. B* **97**, 075426 (2018).
- [20] N. Dashti, M. Misiorny, S. Kheradsoud, P. Samuelsson, and J. Splettstoesser, *Phys. Rev. B* **100**, 035405 (2019).
- [21] C. Grenier, J. Dubois, T. Jullien, P. Roulleau, D. C. Glatli, and P. Degiovanni, *Phys. Rev. B* **88**, 085302 (2013).
- [22] C. Wahl, J. Rech, T. Jonckheere, and T. Martin, *Phys. Rev. Lett.* **112**, 046802 (2014).
- [23] D. Ferraro, B. Roussel, C. Cabart, E. Thibierge, G. Fève, C. Grenier, and P. Degiovanni, *Phys. Rev. Lett.* **113**, 166403 (2014).
- [24] H. Kamata, N. Kumada, M. Hashisaka, K. Muraki, and T. Fujisawa, *Nat. Nanotechnol.* **9**, 177 (2014).
- [25] V. Freulon, A. Marguerite, J.-M. Berroir, B. Plaçais, A. Cavanna, Y. Jin, and G. Fève, *Nat. Commun.* **6**, 6854 (2015).
- [26] D. Dasenbrook and C. Flindt, *Phys. Rev. B* **92**, 161412(R) (2015).
- [27] W. Belzig and M. Vanevic, *Physica E: Low-dimensional Systems and Nanostructures* **75**, 22 (2016).
- [28] L. Vannucci, F. Ronetti, J. Rech, D. Ferraro, T. Jonckheere, T. Martin, and M. Sasseti, *Phys. Rev. B* **95**, 245415 (2017).
- [29] J. Rech, D. Ferraro, T. Jonckheere, L. Vannucci, M. Sasseti, and T. Martin, *Phys. Rev. Lett.* **118**, 076801 (2017).
- [30] Y. Yin, *J. Phys.: Condens. Matter* **30**, 285301 (2018).
- [31] F. Ronetti, L. Vannucci, D. Ferraro, T. Jonckheere, J. Rech, T. Martin, and M. Sasseti, *Phys. Rev. B* **98**, 075401 (2018).
- [32] M. Vanević, J. Gabelli, W. Belzig, and B. Reulet, *Phys. Rev. B* **93**, 041416(R) (2016).
- [33] M. Vanević and W. Belzig, *Phys. Rev. B* **86**, 241306(R) (2012).
- [34] R. Bisognin, A. Marguerite, B. Roussel, M. Kumar, C. Cabart, C. Chapdelaine, A. Mohammad-Djafari, J.-M. Berroir, E. Bocquillon, B. Plaçais, A. Cavanna, U. Gennser, Y. Jin, P. Degiovanni, and G. Fève, *Nat. Commun.* **10**, 3379 (2019).
- [35] L. D. Landau, *Sov. Phys. JETP* **3**, 920 (1957).
- [36] D. Pines and P. Nozières, *The Theory of Quantum Liquids* (CRC Press, Boca Raton, FL, 2018).
- [37] D. A. Ivanov, H. W. Lee, and L. S. Levitov, *Phys. Rev. B* **56**, 6839 (1997).
- [38] C. Grenier, R. Hervé, E. Bocquillon, F. D. Parmentier, B. Plaçais, J. M. Berroir, G. Fève, and P. Degiovanni, *New J. Phys.* **13**, 093007 (2011).
- [39] G. Haack, M. Moskalets, J. Splettstoesser, and M. Büttiker, *Phys. Rev. B* **84**, 081303(R) (2011).
- [40] B. Roussel, C. Cabart, G. Fève, and P. Degiovanni, *PRX Quantum* **2**, 020314 (2021).
- [41] E. Bocquillon, V. Freulon, F. D. Parmentier, J.-M. Berroir, B. Plaçais, C. Wahl, J. Rech, T. Jonckheere, T. Martin, C. Grenier, D. Ferraro, P. Degiovanni, and G. Fève, *Ann. Phys.* **526**, 1 (2014).
- [42] D. Dasenbrook, J. Bowles, J. B. Brask, P. P. Hofer, C. Flindt, and N. Brunner, *New J. Phys.* **18**, 043036 (2016).
- [43] D. C. Glatli and P. S. Roulleau, *Phys. Status Solidi B* **254**, 1600650 (2016).
- [44] C. Bäuerle, D. C. Glatli, T. Meunier, F. Portier, P. Roche, P. Roulleau, S. Takada, and X. Waintal, *Rep. Prog. Phys.* **81**, 056503 (2018).
- [45] E. Olofsson, P. Samuelsson, N. Brunner, and P. P. Potts, *Phys. Rev. B* **101**, 195403 (2020).
- [46] L. S. Levitov, H. Lee, and G. B. Lesovik, *J. Math. Phys.* **37**, 4845 (1996).
- [47] D. C. Glatli and P. Roulleau, *Phys. Rev. B* **97**, 125407 (2018).
- [48] M. Moskalets, *Phys. Rev. Lett.* **117**, 046801 (2016).
- [49] P. P. Hofer and C. Flindt, *Phys. Rev. B* **90**, 235416 (2014).
- [50] B. Gaury and X. Waintal, *Nat. Commun.* **5**, 3844 (2014).
- [51] D. Dasenbrook and C. Flindt, *Phys. Rev. B* **93**, 245409 (2016).
- [52] C. Grenier, R. Hervé, G. Fève, and P. Degiovanni, *Mod. Phys. Lett. B* **25**, 1053 (2011).
- [53] M. Moskalets, *Phys. Rev. B* **91**, 195431 (2015).
- [54] Y. Yin, *J. Phys.: Condens. Matter* **31**, 245301 (2019).
- [55] X. K. Yue and Y. Yin, *Phys. Rev. B* **99**, 235431 (2019).
- [56] M. Moskalets, *Scattering Matrix Approach to Non-Stationary Quantum Transport* (Imperial College Press, London, 2011).
- [57] M. H. Pedersen and M. Büttiker, *Phys. Rev. B* **58**, 12993 (1998).
- [58] T. Martin and R. Landauer, *Phys. Rev. B* **45**, 1742 (1992).
- [59] D. Glatli and P. Roulleau, *Phys. E (Amsterdam)* **76**, 216 (2016).
- [60] T. Brandes, *Ann. Phys.* **17**, 477 (2008).
- [61] M. Albert, C. Flindt, and M. Büttiker, *Phys. Rev. Lett.* **107**, 086805 (2011).

- [62] M. Albert, G. Haack, C. Flindt, and M. Büttiker, *Phys. Rev. Lett.* **108**, 186806 (2012).
- [63] P. P. Hofer, D. Dasenbrook, and C. Flindt, *Phys. E (Amsterdam)* **82**, 3 (2016).
- [64] E. Potanina and C. Flindt, *Phys. Rev. B* **96**, 045420 (2017).
- [65] M. Vanević, Y. V. Nazarov, and W. Belzig, *Phys. Rev. Lett.* **99**, 076601 (2007).
- [66] C. W. J. Beenakker, M. Titov, and B. Trauzettel, *Phys. Rev. Lett.* **94**, 186804 (2005).
- [67] D. Dasenbrook, C. Flindt, and M. Büttiker, *Phys. Rev. Lett.* **112**, 146801 (2014).